RFA for Solar/Geothermal Hybrid Thermal Energy Storage Modeling

Cooperative Research and Development Final Report

CRADA Number: CRD-16-646

NREL Technical Contact: Guangdong Zhu

NREL is a national laboratory of the U.S. Department of Energy
Office of Energy Efficiency & Renewable Energy
Operated by the Alliance for Sustainable Energy, LLC

This report is available at no cost from the National Renewable Energy Laboratory (NREL) at www.nrel.gov/publications.

CRADA Report
NREL/TP-5500-71756
June 2018

Contract No. DE-AC36-08GO28308

NOTICE

This work was authored by the National Renewable Energy Laboratory, operated by Alliance for Sustainable Energy, LLC, for the U.S. Department of Energy (DOE) under Contract No. DE-AC36-08GO28308. Funding provided by USDOE Office of Energy Efficiency and Renewable Energy, Building Technologies Office. The views expressed in the article do not necessarily represent the views of the DOE or the U.S. Government.

This report is available at no cost from the National Renewable Energy Laboratory (NREL) at www.nrel.gov/publications.

U.S. Department of Energy (DOE) reports produced after 1991 and a growing number of pre-1991 documents are available free via www.OSTI.gov.

Cover Photos by Dennis Schroeder: (left to right) NREL 26173, NREL 18302, NREL 19758, NREL 29642, NREL 19795.

NREL prints on paper that contains recycled content.

Cooperative Research and Development Final Report
Report Date: March 3, 2018

In accordance with Requirements set forth in the terms of the CRADA agreement, this document is the final CRADA report, including a list of Subject Inventions, to be forwarded to the DOE Office of Science and Technical Information as part of the commitment to the public to demonstrate results of federally funded research.

Parties to the Agreement: Combined Power LLC, dba Hyperlight Energy

CRADA number: CRD-16-646

CRADA Title: RFA for Solar/Geothermal Hybrid Thermal Energy Storage Modeling

Joint Work Statement Funding Table showing DOE commitment:

Estimated Costs	**NREL Shared Resources** a/k/a Government In-Kind
Year 1	$188,000.00
TOTALS	$188,000.00

Abstract of CRADA Work:

Hyperlight Energy is an innovative concentrated solar power (CSP) company whose business charter is to commercialize a disruptively low-cost, CSP collector system that is ultimately for providing heat for solar thermal/geothermal hybrid power plants, process heat applications (e.g., enhanced oil recovery), and solar thermal power generation. Hyperlight's CSP collector system utilizes a linear Fresnel reflector (LFR) configuration. This LFR configuration consists of mirrors mounted in low-cost, precision plastic extrusions, which are integrated into raft assemblies and floated on low-cost, sealed waterbeds. Hyperlight's CSP collector technology has been developed under private equity investment, government grant and commercial funding. Hyperlight has been awarded a $1.5-million DOE COLLECTS contract with an additional $1.6 million in matched funds from private investment and the California Energy Commission. This DOE project will support the final steps of product development for bulk commercialization and deployment of the Hyperlight CSP collector system. The work will culminate in a final operational deployment at a commercially relevant site. Several such site options are currently under evaluation, including two geothermal sites.

Hyperlight identified a very low-cost way to put renewable energy electrons on the grid at peak times, upgrading underutilized geothermal plants with Hyperlight's low cost CSP and thermal energy storage (TES). While Hyperlight's CSP collector work is maturing quickly for commercial pilot launch, an optimal TES system for solar thermal/geothermal hybridization needs to be evaluated and ultimately developed so Hyperlight can develop commercial retrofit projects at a scale of hundreds of megawatts of renewable energy power output at sites across the United States, followed by greenfield projects in a multi-GW sized market.

This report is available at no cost from the National Renewable Energy Laboratory (NREL) at www.nrel.gov/publications

Summary of Research Results:

Under this Small Business Voucher (SBV) agreement, the National Renewable Energy Laboratory (NREL) has supported Hyperlight Energy in the following areas: (1) ensuring that bundling geothermal and solar thermal energy with thermal energy storage for time-shifting to more profitable periods of time on the grid remains within the infrastructure capabilities of the geothermal plants and (2) helping assess and evaluate candidate lower temperature (250C–395C) thermal storage options.

Further, NREL and Hyperlight successfully engaged Coso Operating Company (Coso) that is operating a geothermal power plant with a capacity of 270 MWe. After entering into a non-disclosure agreement, Coso provided valuable operation data to NREL for the model validation.

Specifically, NREL and the team have successfully performed the following tasks:

Task 1: System Power Generation Modeling

In this task, NREL developed a combined solar thermal/geothermal/thermal storage plant model for purposes of helping to ultimately place thermal power flow requirements (charging and discharging temporal profiles) on the thermal storage system.

Task 2. Preliminary Thermal Storage Evaluation

In this task, NREL populated an initial set of thermal storage media candidates based on temperature requirements, cost, and technology maturity. NREL also conducted detailed analysis to screen thermal storage options that are not strong contenders for the augmented geothermal requirements.

Task 3: Assist in Evaluating Utility Scale Geothermal Resource Constraints

In this task, NREL and the project team performed annual performance analysis and economic analysis to evaluate feasibility of the proposed geothermal/solar hybrid system. NREL also compared the hybrid design with thermal storage with the PV + battery option and showed the superior economic performance of the proposed solar hybridization configuration with thermal storage.

An NREL technical report concluding detailed analysis results is pending for publication and a journal manuscript has been submitted to the journal Applied Energy as well. The journal manuscript is attached for the reference.

Subject Inventions Listing: None

ROI #: None

Responsible Technical Contact at Alliance/NREL: Guangdong Zhu; Guangdong.zhu@nrel.gov

Name and Email Address of POC at Company: Greg Mungas, greg.mungas@hyperlightenergy.com

DOE Program Office: Solar Energy Technology

This report is available at no cost from the National Renewable Energy Laboratory (NREL) at www.nrel.gov/publications

A hybrid power plant combining geothermal, concentrating solar, and thermal energy storage provides dispatchability and increased power generation

Joshua D. McTigue [1], Jose Castro [2], Greg Mungas [3], Nick Kramer [3], John King [3], Craig Turchi [1], Guangdong Zhu [1*]

[1] National Renewable Energy Laboratory, 15013 Denver West Parkway, Golden, CO, 80401, USA

[2] Coso Operating Company, CA, USA

[3] Hyperlight Energy, Ltd., San Diego, CA, USA

[*] Corresponding author. Email: Guangdong.Zhu@nrel.gov Tel: +1 303-275-4497

Highlights

- Retrofitting a geothermal plant with concentrating solar power increases electricity production.
- The hybrid plant converts solar thermal energy to electricity with an efficiency of 24%.
- Thermal energy storage provides dispatchable power generation.
- The hybrid plant LCOE is competitive with photovoltaic arrays with battery storage.

Abstract

Geothermal power plants often deploy less than their full power capacity due to declining geothermal resources. Integrating heat from a concentrating solar field increases the power output at low cost. This article considers five methods of solar heat addition in a double-flash geothermal plant. The most promising solution converts solar heat into electrical work with an efficiency of 24.3%. The economic feasibility and optimal sizing of the solar field and thermal stores are evaluated. A hybrid plant that increases power generation from 22 to 24 MW_e has a Levelized Cost of Electricity (LCOE) of 0.07 ± 0.01 $/kWh. Adding four hours of storage increases the LCOE to 0.08 ± 0.01 $/kWh, while an equivalent photovoltaic system with battery storage costs 0.11 ± 0.02 $/kWh. If the dispatchability that thermal storage provides is rewarded with higher electricity prices, calculations indicate storage becomes an attractive investment when discharged energy receives 1.75 times the going rate for electricity.

Keywords

Concentrating solar power, thermal energy storage, geothermal power, retrofit, levelized cost of energy, and hybrid power generation.

1. Motivation

Geothermal resources typically experience a reduction in the temperature, pressure, or mass flow rate of its production fluids over time, leading to decreased power generation and underutilized equipment. If a Power Purchase Agreement exists, plant operators may be subject to additional fees for not producing

This report is available at no cost from the National Renewable Energy Laboratory (NREL) at www.nrel.gov/publications

agreed amounts of power [1]. The extent of any resource decline is unique to that geothermal field. A study of geothermal power plants in California and Nevada found that flash plants typically experienced a temperature decrease of 0.8% per year, while the value was 0.5% for binary plants [2]. Underperforming plants may be brought back to full capacity by the addition of thermal heat. The unused capacity of the geothermal plant provides an opportunity to install a concentrating solar plant at reduced cost since investment in a power unit and condenser is not required. Integrating thermal storage provides the plant with flexibility and dispatchability.

The first geothermal/solar hybrid plant was developed at the Stillwater Power Plant in Nevada and began operating in 2015. A solar field of parabolic trough collectors supplies 17 MW_{th} of thermal power to the 33 MW_e geothermal power plant and augments production by 2 MW_e [3]. The plant also includes a 26-MW_e photovoltaic solar array, which offsets the decrease in power generation that occurs at high ambient temperatures [4]. Operators of the 13.2-MW_e Gümüşköy geothermal binary plant in Turkey aimed to reduce the detrimental impact of high ambient temperatures by using solar heat to augment generation [5]. Tests were conducted with a 200-kW_{th} array of parabolic trough collectors in 2014. Most previous studies have investigated hybrid plants with parabolic trough collectors and have not implemented thermal storage. Researchers have investigated systems using binary plants [6]–[8] and single-/double-flash plants [9]–[12].

This article concentrates on the integration of solar heat into a double-flash geothermal power plant, where production fluids are flashed and the resulting steam powers a steam turbine. Hybrid plants require good solar and geothermal resources, and Figure 1 indicates that the most suitable locations in the United States are the Western states and are primarily dependent on the geothermal resource location.

The installed geothermal capacity in the United States is 3134 MW_e, most of which is concentrated in California and Nevada (see Figure 1). Flash plants comprise 29% of U.S. geothermal capacity and, notably, 90% of U.S. flash plant capacity is over 25 years old, indicating that many existing plants may be experiencing the effects of resource decline. The opportunity to explore resource decline mitigation currently exists in the United States, and the results may have benefits internationally because flash plants make up 65% of the world's total installed capacity of 11 929 MW_e.

In this article, several methods of integrating solar heat into a geothermal power plant will be investigated. A thermodynamic model of the system is developed, and annual calculations are undertaken to evaluate the Levelized Cost of Electricity (LCOE). The hybrid plant LCOE is compared to an equivalent photovoltaic array with batteries. The hybrid system includes two-tank, liquid thermal-energy storage that is a technologically deployable storage system. Alternative storage systems that are more compact and cost effective are also considered.

This report is available at no cost from the National Renewable Energy Laboratory (NREL) at www.nrel.gov/publications

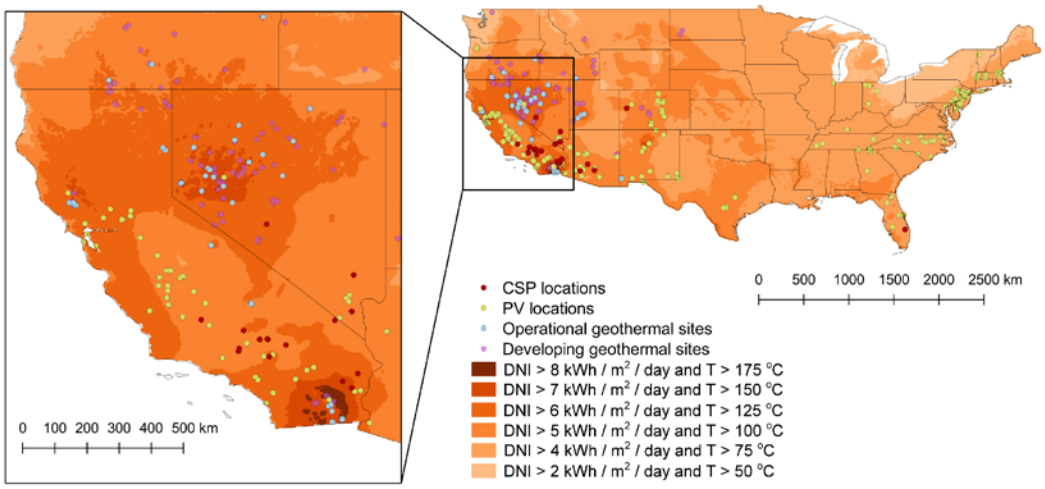

Figure 1: Potential locations for geothermal-solar hybrid plants and design requirements; map of the United States showing locations of high solar irradiance and geothermal temperatures at a depth of 3000 m. Data from National Solar Radiation Database [55].

2. Modeling of the hybrid system

The geothermal plant is a double-flash power plant, where steam produced from geothermal fluids in a flash tank is diverted to the high-pressure stage of a steam turbine. The brine enters a second flash tank, and the produced steam is injected into the low-pressure steam turbine stage. The power plant is based on the units at the Coso geothermal field and was modelled in the IPSEpro heat-balance software, developed by SimTech [13]. Design and off-design performance were validated against data provided by the Coso Operating Company that operates a double-flash geothermal plant in China Lake, California.

The hybrid plant consists of a double-flash geothermal power plant and an array of mirrors to concentrate sunlight; two liquid tanks contain the heat transfer fluid and are used as thermal storage.

2.1 Geothermal production fluids

The geothermal well produces fluid that follows a characteristic curve. The fluid pressure is inversely related to the mass-flow rate and is assumed to follow a choked-flow correlation, as proposed by DiPippo [14]. However, rather than using DiPippo's cubic correlation that has an inflection point at high pressures, data points were tabulated (see Table 1). Intermediate points are evaluated with cubic-spline interpolation.

The values of p_{max} and $\dot{m}_{max}$ were set at p_{max} = 30 bar, $\dot{m}_{max}$ = 125 kg/s to match the design point requirements of the geothermal plant. The current operating point of the power plant was obtained by reducing the maximum mass flow rate to $\dot{m}_{max}$ = 112 kg/s. The geothermal fluid was assumed to have a specific enthalpy of 1500 kJ/kg, which is in line with typical enthalpies observed at Coso. The salt content of geothermal production fluids is low, and the fluid can therefore accurately be modelled using water properties.

This report is available at no cost from the National Renewable Energy Laboratory (NREL) at www.nrel.gov/publications

Table 1: Pressure-mass flow characteristic for a geothermal well

$\dot{m} / \dot{m}_{max}$	p / p_{max}
0.000	1.00
0.135	0.99
0.339	0.98
0.508	0.96
0.678	0.90
0.763	0.80
0.950	0.55
0.980	0.38
0.990	0.19
1.000	0.00

2.2 Steam turbine

Off-design behavior of the steam turbine is modelled using Stodola's ellipse, which relates the mass flow rate and the inlet and outlet pressures through [15]:

$$\dot{m}\left(\sqrt{T_{01}}\right) / \, p_{01} = k\left[1-\left(p_{0e} / \, p_{01}\right)^2\right]^{1/2} \tag{1}$$

Where $\dot{m}$ is the mass flow rate, T_{01} is the inlet temperature, p_{01} is the inlet pressure, p_{0e} is the outlet pressure, and k is a constant of proportionality. Assuming that k is constant for all cases, off-design performance may be related to design performance with the following relation [16]:

$$\frac{\dot{m}}{\dot{m}_{\text{ref}}}\left(\sqrt{\frac{T_{01}}{T_{01\,,\,\text{ref}}}}\right)\frac{p_{01\,,\,\text{ref}}}{p_{01}} = \frac{\left[1-\left(p_{0e} / \, p_{01}\right)^2\right]^{1/2}}{\left[1-\left(p_{0e,\,\text{ref}} / \, p_{01\,,\,\text{ref}}\right)^2\right]^{1/2}} \tag{2}$$

A variety of physical mechanisms lead to entropy generation in the steam turbine, as described in [17]. Rather than undertaking detailed stage-by-stage calculations, stages are grouped into sections and correlations of each section efficiency are used to predict turbine performance. The correlations are based on experimental results from turbine units and stage-by-stage calculations. The correlations were originally developed by Spencer-Cotton-Cannon [18], [19]; computer code was developed in [20] and implemented in IPSEpro.

Off-design performance of the steam turbine was validated against operational data provided by Coso Operating Company.

The steam turbine is primarily operated with 'sliding pressure' control, where inlet pressure floats in response to the varying mass flow rate in accordance with Stodola's ellipse to maintain a constant volumetric flow rate. It is assumed that the outlet pressure is fixed by the condenser pressure and is constant. The condenser is water cooled and its pressure therefore does not vary significantly with atmospheric pressure.

This report is available at no cost from the National Renewable Energy Laboratory (NREL) at www.nrel.gov/publications

The turbine is constrained to a maximum inlet pressure 10% greater than the design value. If more mass is available, a valve before the turbine is throttled to maintain the inlet pressure at its maximum value (which leads to larger losses). The excess steam is flashed in the second flash tank and more steam enters the low-pressure turbine stage.

2.3 Flash tanks

The flash tanks are assumed to be isenthalpic and to separate the vapor and liquid with 100% efficiency. In practice, typical separation efficiencies are of the order of 99.9% [21].

2.4 Heat exchanger

Solar heat is transferred to the geothermal system in a heat exchanger. The heat exchangers are modelled using a simple energy balance, such that

$$\dot{m}_c \left(h_{c\,,\,\mathrm{out}} - h_{c\,,\,\mathrm{in}} \right) = \dot{m}_h \left(h_{\mathrm{h}\,,\,\mathrm{in}} - h_{\mathrm{h}\,,\,\mathrm{out}} \right) \tag{3}$$

where h is the enthalpy and is a function of temperature and pressure. The cold inlet temperature $T_{c\,,\,\mathrm{in}}$ is known (from the geothermal model) and the cold outlet temperature $T_{c\,,\,\mathrm{out}}$ and pressure are specified. The hot outlet temperature is given by assuming $T_{h\,,\,\mathrm{out}} = T_{c\,,\,\mathrm{in}} + \Delta T_c$, where ΔT = 25°C. The hot inlet temperature is specified; two cases are examined in this paper, $T_{h\,,\,\mathrm{in}}$ = 300°C and $T_{h\,,\,\mathrm{in}}$ = 400°C.

It is assumed that the solar field heats up the HTF to a constant temperature, $T_{h\,,\,\mathrm{in}}$, which is achieved by varying the mass flow rate of fluid through the solar collectors.

2.5 Solar field model

The available solar resource was given by TMY3 (Typical Meteorological Year) data for China Lake, California, and was obtained from the System Advisor Model (SAM) [22].

The solar field uses Linear Fresnel Reflector (LFR) technology to concentrate sunlight. The LFR arrays are based on those designed by Hyperlight Energy Ltd., and the optical and thermal efficiencies are based on Hyperlight Energy's calculations and experiments.

The optical efficiency η_{opt} of an LFR array may be written as

$$\eta_{\mathrm{opt}} = \gamma \rho \tau \alpha \cdot \mathrm{IAM}\left(\theta_{\perp}, \theta_{\parallel} \right) \tag{4}$$

where γ is the intercept factor, ρ is the reflectance, τ is the transmittance, α is the average absorptance of the receiver surface, IAM is the Incident angle modifier, and $\theta_{\perp}, \theta_{\parallel}$ are the transversal and longitudinal incidence angles respectively. The incidence angles are calculated using the FirstOPTIC method developed in [23]. The IAM is a function of these angles and further details are provided in [24].

Heat transfer losses from the solar receiver are calculated using the empirical correlations similar to those in [25] and has the form:

This report is available at no cost from the National Renewable Energy Laboratory (NREL) at www.nrel.gov/publications

$$\phi = 0.141\ T_{\text{abs}} + 6.48 \text{ x } 10^{-9}\ T^4{}_{\text{abs}} \tag{5}$$

Where ϕ is the heat loss in W/m, and T_{abs} is the temperature in °C. However, the correlations have been updated to be more applicable to the LFRs developed by Hyperlight Ltd.

Heat transfer fluid fills the absorber pipe and surrounding pipework in the solar field. The volume of HTF per m^2 of mirror area is calculated as 3.34 x 10^{-3} m^3 / m^2 using dimensions of Hyperlight's LFR array. There is a single absorber tube with a diameter of 90 mm for a pair of basins. The basin supports the mirrors. A basin has a length of 15.2 m and a mirror area of 72.5 m^2. The HTF volume per m^2 of mirror is therefore 6.67 x 10^{-4} m^3 / m^2. This value is then multiplied by a factor of 5 to represent the additional HTF that is required to fill the pipelines.

The size of the solar field is quantified using the 'solar multiple,' σ. A CSP field with a solar multiple of 1 can provide the rated thermal capacity when the Direct Normal Irradiance (DNI) is at its maximum expected value. Increasing the solar multiple proportionally increases the solar field size and its power output. A CSP field with a solar multiple of 2 will have double the area, for example:

2.6 Thermal storage model

The storage system is composed of two tanks that store the liquid HTF at different temperatures. In this analysis, the cold store is at 190°C and the hot store is at 300°C or 400°C, depending on the choice of HTF.

Each store is governed by a mass and energy balance, which may be written as

$$\frac{\mathrm{d}\dot{m}}{\mathrm{d}t} = \dot{m}_{\text{in}} - \dot{m}_{\text{out}} \tag{6}$$

$$\frac{\mathrm{d}\left(\dot{m}h\right)}{\mathrm{d}t} = \dot{m}_{\text{in}} h_{\text{in}} - \dot{m}_{\text{out}} h_{\text{out}} \tag{7}$$

where $\dot{m}$ is the mass flow rate, h is the enthalpy, t is time, and *in* and *out* represent the flows into and out of the store, respectively.

The volume of the containers required to store a quantity of energy E between two tanks at different volumes is given by

$$E = \left(\beta \rho_f V c_p T\right)_h - \left(\beta \rho_f V c_p T\right)_c \tag{8}$$

where ρ_f is the fluid density, V is the volume, c_p is the specific heat capacity, T is the temperatures, and β is an additional factor, which accounts for the fact that the tanks should be slightly oversized. The subscripts h and c represent the hot and cold store, respectively. The storage should deliver a power P for τ_d hours to have stored E. The energy is also given by

$$E = P\tau = \dot{m}\left(c_{p,h} T_h - c_{p,c} T_c\right)\tau_d \tag{9}$$

This report is available at no cost from the National Renewable Energy Laboratory (NREL) at www.nrel.gov/publications

The volume of each store can then be found from

$$V = \frac{\dot{m}\tau_d}{\beta\rho_f} \tag{10}$$

HTF thermal properties were collected from manufacturers typically included specific heat capacity, density, vapor pressure, and viscosity. Properties vary smoothly with temperature, so intermediate values may be found by cubic spline interpolation. The enthalpy h and entropy s were evaluated using

$$h = \int_{T_1}^{T_2} c_p \, \mathrm{d}T \; ; \; s = \int_{T_1}^{T_2} \frac{c_p}{T} \mathrm{d}T \tag{11}$$

Water properties are calculated using REFPROP and CoolProp software.

2.7 Hybrid plant efficiencies

The first-law thermodynamic efficiency of the hybrid system may be written as

$$\eta_1 = \frac{\dot{W}_{\mathrm{net}}}{\dot{Q} + \dot{Q}_{\mathrm{sol}}} \tag{12}$$

where $\dot{W}_{net}$ is the net work output, $\dot{Q}$ is the heat addition across the power block when no solar heat is added, and $\dot{Q}_{\mathrm{sol}}$ is the solar heat addition. Another useful metric is the solar thermal conversion efficiency, which is defined as the net increase in electrical work divided by the solar heat input.

$$\eta_{\mathrm{sol}} = \frac{\dot{W}_{net} - \dot{W}_o}{\dot{Q}_{\mathrm{sol}}} \tag{13}$$

where $\dot{W}_o$ is the work output when no solar heat is added.

3. Comparison of hybrid plant configurations

Concentrating solar and thermal storage are added to a double-flash geothermal power plant, which is assumed to be running at 75% of its operating capacity. The off-design behavior is validated against operational data provided by the Coso Operating Company for units located at the Naval Air Weapons Base in China Lake, California [26]. Figure 2a indicates the layout of a double-flash geothermal power plant with a two-stage steam turbine, and the design point and current operating conditions are given in Table 2. The hybrid plant has thermal storage in the form of two liquid tanks, which contain the same heat transfer fluid as used in the solar collectors. This is the most readily deployable storage solution available and has been used previously in several CSP installations [27].

Heat generated by the solar field can be added at numerous points in the geothermal system. The optimal hybrid configuration will depend on the location of components, the properties of the geothermal fluids, and the performance of the plant. One of the first hybrid plants was proposed in 1979 and it used geothermal heat for feedwater heating and solar heat to boil water for use in a steam turbine [28]. These

This report is available at no cost from the National Renewable Energy Laboratory (NREL) at www.nrel.gov/publications

hybrid plants demonstrated no economic advantages over stand-alone geothermal plants. However, CSP prices have dropped significantly and it is appropriate to reconsider this technology. Four methods for adding solar heat to the Ahuachapán geothermal field in El Salvador to increase the power output by 2 MW_e to 97 MW_e have been considered [10], [11]. Heating the brine directly from the production well required a large heat exchanger and was ruled out. A method that was successfully tested involved heating brine from the first separator and directing the generated steam into the high-pressure turbine.

Table 2: Design and off-design inputs and performance data used to model a two-stage, steam-turbine unit

		Design conditions		Current operating conditions	
		High pressure	*Low pressure*	*High pressure*	*Low pressure*
Mass flow	kg s^{-1}	48.0	25.0	43.8	7.1
Temperature	°C	169.2	132.5	159.8	98.3
Inlet pressure	bar	6.3	1.4	5.7	0.95
Gross power	MW_e	29.6		22.5	
Net power	MW_e	29.4		22.2	
Efficiency	%	19.7		16.9	

Cardemil et al. compared two locations of solar-heat addition in single- and double-flash plants in the Atacama Desert, Chile [12]. After the flash tank, the solar field could superheat the steam or evaporate the brine. Using 2nd Law analysis, it was concluded that superheating the steam was slightly more effective because the turbine operated more efficiently with dry steam. Double-flash systems were also found to be preferable to single-flash plants.

The impact of adding solar heat Q_{sol} in five ways is presented in Figure 2b–e. These figures indicate that Q_{sol} increases power output and first law efficiency η_1, while the solar-conversion efficiency η_{sol} is fairly constant. Increasing Q_{sol} increases the steam flow rate that is delivered to the high-pressure turbine, thereby increasing the inlet pressure. However, the characteristic curve of the geothermal well has mass-flow rate inversely related to pressure [14]. Increasing the turbine inlet pressure therefore requires a lower mass flow rate from the geothermal field, thereby potentially increasing the lifetime of the geothermal resource. The additional mass required by the turbine is then supplied by recirculating fluid or increasing steam generation, as described below.

The turbine is operated with 'sliding-pressure' control, whereby the inlet pressure and mass vary in response to changes in the flow from the wells and the solar field. Above the maximum turbine inlet pressure, the turbine inlet is throttled and a noticeable kink is apparent in the trendlines of Figure 2b-e. The power continues to increase, albeit at a slower rate, but η_{sol} drops significantly, as does η_1.

The four configurations are:

INJ—In normal operation of the geothermal plant, unflashed brine is pressurized to 15 bars and re-injected into the ground at ~104°C. A fraction of this brine is heated by the solar field until becoming saturated liquid and is then mixed with the production fluids. This configuration shows the poorest performance with the power input increasing 0.16 MW_e per MW_{th} heat addition. The 1st law efficiency η_1

This report is available at no cost from the National Renewable Energy Laboratory (NREL) at www.nrel.gov/publications

decreases as solar heat is added because the solar-conversion efficiency, η_{sol} is less than the 1st law efficiency when $Q_{sol} = 0$ (proof in Appendix A). Increasing the reheat brine temperature improves performance slightly by increasing the specific enthalpy of the mixed fluid.

INJ2—Evaporating the injection brine to a vapor fraction of 50% improves the performance compared to INJ. The solar-conversion efficiency increases to 22.5% from around 17% and η_1 increases with heat addition. However, this approach may result in increased mineral deposition in the pipes and heat exchanger. Using a shell-and-tube heat exchanger with the brine inside the tubes will make it easier to clean, although phase change normally occurs on the shell side.

COND—Water leaves the condenser at ~38°C and 0.1 bar and may be evaporated without scaling issues. Saturated vapor is injected directly into the high-pressure turbine stage and its temperature is set by the turbine inlet pressure. Alternatively, the turbine exhaust steam could be heated, which would increase the recirculated mass for the same heat addition because the exhaust is hotter (~46 °C) than the condenser water. However, the exhaust is a low pressure (0.1 bar) two-phase mixture and compressing this fluid to the required turbine inlet pressure (6 bar) necessitates a considerable work input and a two-phase pump. Furthermore, an isentropic compression would increase the fluid temperature to 550°C, thereby rendering the solar field redundant.

PRE—The two-phase production fluids are heated directly, thereby increasing their vapor fraction. This method sees the highest increase in power output per unit heat addition with $\eta_{sol} = 25\%$. However, evaporation can lead to an increased rate of scaling [29], although the precipitation may be delayed by the introduction of H_2SO_4 [30]. A larger heat exchanger may also be required due to the larger flow rates. For instance, $Q_{sol} = 10$ MW_{th} heats 110.6 kg s^{-1} of production fluids compared to 24.6 kg s^{-1} for INJ and 62.0 kg s^{-1} for FT1.

FT1—Brine leaves the first flash tank (FT1) at ~165°C compared to the FT2 outlet. which is 104°C. Heating FT1 brine therefore recirculates more mass per unit heat addition. This approach has a comparable performance to PRE with $\eta_{sol} = 24.3\%$. Increasing the temperature to which the fluid is heated reduces net power by a small quantity; the increase in enthalpy of the mixed fluid is outweighed by the increased pumping power to keep the fluid saturated. This configuration has the best performance with the least risk of scaling and is investigated further (see below).

This report is available at no cost from the National Renewable Energy Laboratory (NREL) at www.nrel.gov/publications

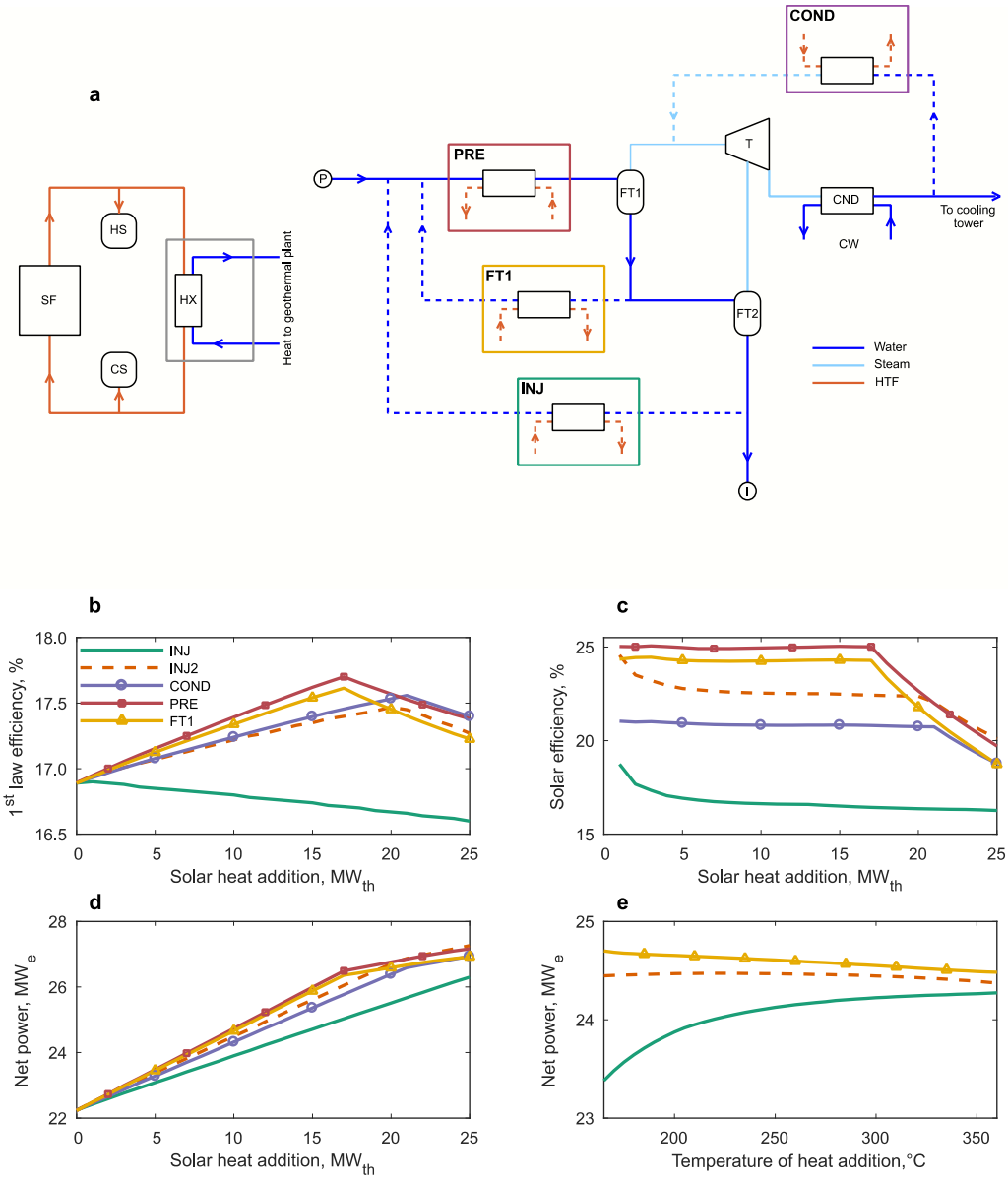

Figure 2: Solar heat can be added at different points in the geothermal power plant. **a**, Schematic of hybrid power plant with solar heat added in five ways: INJ – injection brine is heated to saturation temperature; INJ2 – same as INJ, except fluid is heated until the vapor fraction is 50%; COND – The condensed water is heated; PRE – geothermal production fluids are preheated; FT1 – brine at the first flash tank exit is heated. **b**, Variation of first-law thermal efficiency with the quantity of solar heat addition, Q_{sol}. **c**, Variation of solar-conversion efficiency with Q_{sol}. **d**, Variation of net power with Q_{sol}. e, Variation of net power with the temperature of solar heat addition. *Key:* SF – solar field; HS – hot store; CS – cold store; HX – heat exchanger; P – production well; I – injection well; FT1 – flash tank 1; FT2 – flash tank 2; T – turbine; CND – condenser; CW – cooling water. Valves, pumps etc. are not shown for clarity. In b, c, and d the solar field HTF is heated to 190°C. The HTF cold temperature is set to be 25°C greater than the geothermal inlet fluid.

This report is available at no cost from the National Renewable Energy Laboratory (NREL) at www.nrel.gov/publications

4. Annual simulations

Variations in available solar resource affect the hybrid plant performance. The thermal power delivered by the solar collector is a function of the sun angle, direct normal irradiance (DNI), mirror properties, and temperature of the HTF.

The design point of the hybrid plant has a net power generation of 24.2 MW_e, which is a 2 MW_e increase in the electrical work output of the geothermal plant. This corresponds to a thermal power of 8 MW_{th} for the FT1 configuration. Generating this thermal power requires a solar field with a mirror area of 14159 m^2 at the peak DNI on the summer solstice (973 Wm^{-2}). A solar field of this size has a *solar multiple* $\sigma = 1$. Increasing the solar multiple proportionally increases the solar field size and its power output.

The operating point of the geothermal system with 8 MW_{th} power addition is shown in Table 3. If the solar collectors provide more than 8 MW_{th}, then the excess energy is stored. Once the thermal stores are full, the excess energy is dispatched to the geothermal plant, up to a maximum thermal input of 16 MW_{th}, which corresponds to the point where the inlet pressure to the turbine can no longer be increased and the turbine must be throttled. Beyond this heat input, thermal energy from the solar field is curtailed.

Table 3. Operating point of hybrid plant using FT1 configuration. **The hot store temperature depends on the maximum operating temperature of the HTF. Two cases are investigated in this article*

		HP stage	LP stage
Temperature	°C	162.6	100.0
Pressure	bar	6.10	1.01
Mass flow rate	kg/s	47.2	54.2
Recirculated temperature	°C	162.6	
Recirculated pressure	bar	6.60	
Recirculated mass flow rate	kg/s	147.9	
Cold store temperature	°C	190.0	
Hot store temperature*	°C	300.0/400.0	
Solar thermal energy	MW_{th}	8.0	
Gross power	MW_e	24.5	
Net power	MW_e	24.2	
1st-law efficiency	%	17.3	
Solar thermal conversion efficiency	%	24.3	

This report is available at no cost from the National Renewable Energy Laboratory (NREL) at www.nrel.gov/publications

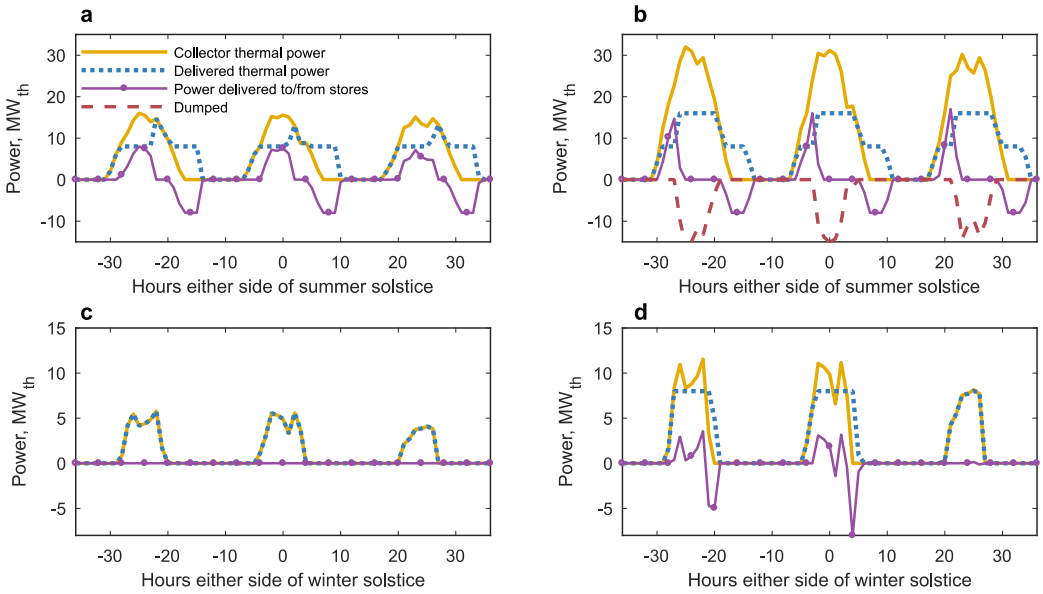

Figure 3: Power flows in the hybrid power plant for the summer solstice and winter solstice. **a**, Summer solstice, solar multiple = 2. **b**, Summer solstice, solar multiple = 4. **c**, Winter solstice, solar multiple = 2. **d**, Winter solstice, solar multiple = 4.

The hourly behavior of the hybrid system is illustrated in Figure 3 for solar multiples of $\sigma = 2$ and 4. Graphs are shown at the summer and winter solstice to show the extreme cases. At $\sigma = 2$, the plant cannot deliver the target thermal power (8 MW_{th}) in the winter solstice and stores are underutilized, discharging only 0.1% of the energy than if they were fully charged and discharged each day, (see

Table 4). The storage utilization is a measure of the capacity factor of thermal stores and is the ratio of the actual energy discharged to the total quantity that could have been dispatched if the stores had been fully charged and discharged once per day.

Solar multiples of 4 are large compared to most current installations. However, the stores are still used to only a small extent throughout the winter, with utilizations of 25% for an 8-hour store. On the other hand, during the summer the stores are fully charged daily with utilizations over 99%. If the stores are full and the geothermal plant cannot accept all the available thermal power, then the power is curtailed, as shown in Figure 3b, which indicates that the solar field is not cost efficient. There is an inherent trade-off in sizing the solar field and thermal stores—large solar fields are required to provide the required power in the winter. However, this leads to an oversupply of energy in the summer, requiring large stores to avoid curtailment. These large stores are then underutilized in the winter.

This report is available at no cost from the National Renewable Energy Laboratory (NREL) at www.nrel.gov/publications

Table 4. Performance of thermal stores in the hybrid plant

		Solar multiple = 2		Solar multiple = 4	
Solar field mirror area	m^2	28,318		56,636	
Annual collector energy	GWh_{th}	28.83		57.66	
Annual increase in electrical energy	GWh_e	6.97		11.37	
Average electricity generated [a]	MWh_e	23.0		23.5	
Average first-law efficiency	%	17.7		18.5	
Capacity factor [b]	%	42.0		67.6	
		Storage		*Storage*	
		4 h	8 h	4 h	8 h
Total energy discharged	GWh_{th}	6.1	7.0	9.7	17.4
Utilization [c]	%	52.4	30.0	83.2	74.6
Average energy discharged (May–Jul)	MWh_{th}/day	30.0	37.7	31.8	63.4
Utilization (May–Jul)	%	*93.4*	*59.0*	*99.3*	*99.0*
Average energy discharged (Nov–Jan)	MWh_{th}/day	0.1	0.1	14.9	15.7
Utilization (Nov–Jan)	%	*0.2*	*0.1*	*46.5*	*24.6*
Total energy curtailed	GWh_{th}	0.0	0.0	10.7	6.7

[a] The average electricity generated per day without solar is 22.2 MW_e.

[b] The capacity factor is defined as the average additional electricity divided by the design value of additional electricity (2 MW_e).

[c] The storage utilization is defined as the total energy discharged divided by the total energy that would have been dispatched if the store had been fully charged and discharged once per day.

5. Levelized Cost of Electricity (LCOE) of the hybrid plant

The levelized cost of electricity (LCOE) is calculated over a 30-year lifetime for various sizes of solar field, storage durations, and HTF temperatures. The levelized cost of electricity is the cost that, if assigned to every unit of electrical energy produced over the lifetime of the plant, will equal the total lifecycle costs when discounted back to the current year [31]. The total lifecycle costs include capital costs and operational and maintenance costs. In the case of the hybrid plant where the power block and geothermal wells already exist, the annual electrical energy is given by the marginal increase in electrical energy above the base rate provided by the geothermal plant.

The LCOE is calculated using the fixed charge rate (FCR) method, where

$$\mathrm{LCOE} = \frac{C_{\mathrm{cap}}\mathrm{FCR} + M}{E} \tag{14}$$

where C_{cap} is the capital cost, M is the annual operational and maintenance costs, E is the annual electricity generation, and FCR is the fixed charge rate. FCR is defined as the revenue per unit of investment that must be collected annually to pay for the carrying charges of the investment. Details of how to calculate the FCR may be found in the [31]. The cost of each component is evaluated using correlations developed from the literature and industry representatives and are presented in Appendix B.

This report is available at no cost from the National Renewable Energy Laboratory (NREL) at www.nrel.gov/publications

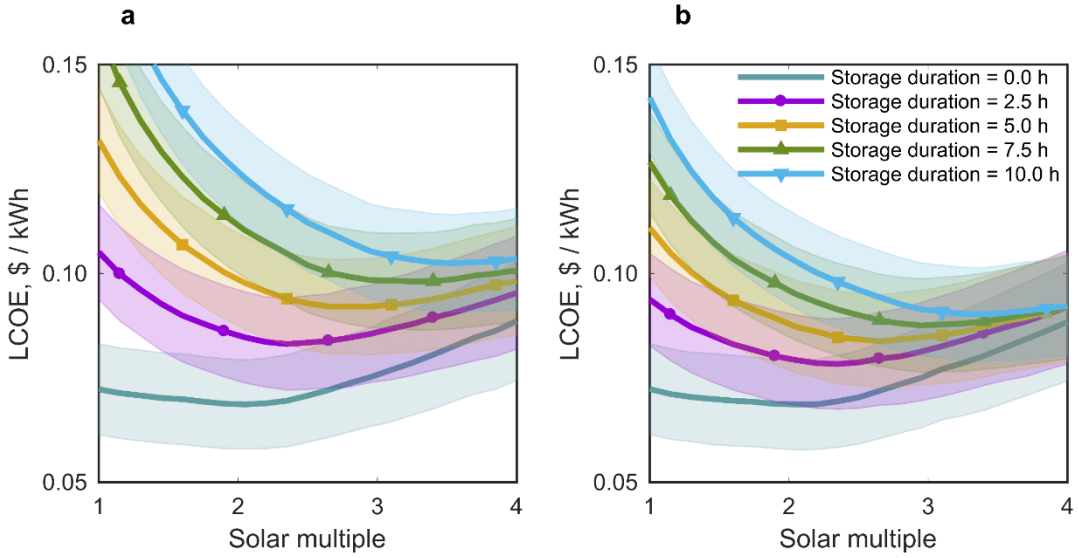

Figure 4: Effect of solar field size and thermal storage sizing on the levelized cost of energy. **a**, The hot thermal store is at 300°C with the Xceltherm 600 mineral oil for storage medium. **b**, The hot thermal store is at 400°C with DPO as the storage medium. The cold store is at 190°C in both cases. The shaded bars indicate the mean LCOE plus/minus one standard deviation.

Figure 4 indicates that larger solar fields reduce the LCOE as more energy is delivered to the hybrid plant over the course of the year. However, the LCOE increases for high solar multiples, due to increased curtailment. Curtailment can be reduced by increasing the storage duration, which explains why the lines begin to converge at large solar multiples.

The choice of heat transfer fluid for the storage media significantly affects the LCOE. Figure 4a illustrates the LCOE of a mineral oil (Xceltherm 600) that has low capital cost (2.5 $/kg), is non-toxic, and has low vapor pressures, so that the stores do not need to be pressurized. The maximum operating temperature of the mineral oil is 300°C.

On the other hand, a synthetic fluid with a maximum operating temperature of 400°C is shown in Figure 4b. This fluid is a eutectic mixture of diphenyl and biphenyl oxides (DPO) (marketed as Dowtherm A, Therminol VP1 and so on.). DPO has more expensive upfront costs (3.1 $/kg) compared to mineral oils. Furthermore, operating at higher temperatures increases the vapor pressure (~10 bar at 400°C), requiring pressurized stores that are more expensive by a factor of ~1.3. DPO is more toxic and less environmentally friendly than mineral oils. Operators may be cautious of storing large volumes of DPO after a fire at the SEGS1 CSP plant in 1999 destroyed 3400m^3 of DPO and caused considerable damage.

The cold tank in both cases has a temperature of 190°C. Increasing the temperature difference between the stores increases the energy density, thereby reducing the storage volume and cost. Figure 4 indicates that this outweighs the impact of using a more expensive HTF and a pressurized vessel. For instance, the LCOE of a system with DPO, $\sigma = 2$, and 4 hours of storage is 0.085 ± 0.011 $/kWh compared to an equivalent plant with mineral oil which costs 0.093 ± 0.011 $/kWh. Using DPO instead of mineral oil reduces the storage capital cost from 60 to 39 $/kWh.

This report is available at no cost from the National Renewable Energy Laboratory (NREL) at www.nrel.gov/publications

Note that the capital cost per unit energy can be calculated in two ways. Literature typically quotes the capital cost per unit energy capacity of the store. However, a more representative value is given by considering the extent to which the store is used—how much energy is discharged over a typical cycle. Table 5 provides the capital cost per unit energy dispatched, which is significantly larger than the capital cost per unit energy capacity. For instance, the DPO store capital cost per unit energy dispatched is nearly double (114.5 $/kWh) the capital cost per unit capacity because of a storage utilization of 52.5%.

Larger thermal stores lead to higher LCOEs, as the total electricity generation remains roughly the same while the investment increases. The LCOE implies that the optimal storage size is zero, as it does not capture the value that storage provides to the plant or the grid by enabling the flexible dispatch of energy [32]. The 'optimal' storage size can be found by considering the capital cost per unit energy discharged on average (see Figure 5). For instance, large stores achieve economies of scale and have low-capital costs per unit *capacity*. However, they are infrequently fully charged, so the capital cost per unit energy dispatch is high. Conversely, small stores are frequently utilized, but have higher capital costs per unit capacity. The 'optimal' storage duration is 3 hours and 10 hours for solar multiples of 2 and 3, respectively, when the storage fluid is DPO.

These graphs illustrate the inherent trade-off in sizing the thermal stores. Efficient use of the storage capacity requires small stores, but cost considerations indicate that larger stores are more cost effective (from a storage perspective). Table 5 compares the economic cost of two solar field sizes with no storage and with the optimal duration of storage, according to the cost per kilowatt-hour dispatched for the DPO stores.

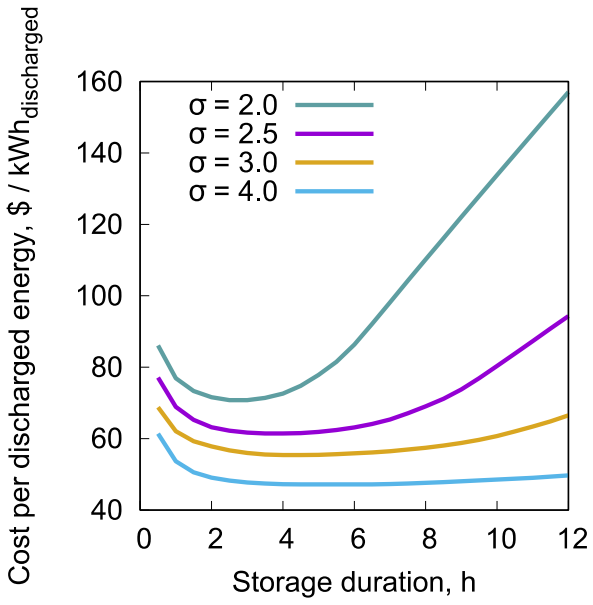

Figure 5: Cost per unit energy dispatched of two-tank thermal storage using DPO. The hot store is at 400°C, the cold store is at 190°C, and the system discharges at 8 MWth

This report is available at no cost from the National Renewable Energy Laboratory (NREL) at www.nrel.gov/publications

Table 5. Hybrid plant economics for different solar multiples, with and without optimally sized stores

		Solar multiple = 2		Solar multiple = 3	
		0 h (mineral)	3 h (synthetic)	0 h (mineral)	10 h (synthetic)
Total energy	GWh_{th}	28.8	28.8	43.2	43.2
Additional electricity	GWh_e	6.98	6.97	9.34	10.42
Solar field cost	M$	4.25	4.25	6.37	6.37
Solar field HTF	M$	0.230	0.286	0.345	0.430
Pump cost	M$	0.211	0.211	0.211	0.211
HX cost	M$	0.060	0.046	0.060	0.046
HTF cost	M$	0.0	0.595	0.0	1.982
Storage cost	M$	0.0	0.397	0.0	0.777
Capital cost	M$	4.750	5.785	6.986	9.816
Storage cost	$ / kWh	0.0	41.3	0.0	34.5
Storage utilization	%	0.0	57.0	0.0	57.9
LCOE	$ / kWh	0.069 ± 0.011	0.081 ± 0.011	0.076 ± 0.012	0.091 ± 0.011
IRR	%	7.73 ± 3.24	5.72 ± 2.57	6.58 ± 3.05	4.55 ± 2.34

6. Comparison with PV + Storage

The economic feasibility of the hybrid plant is compared to a solar photovoltaic (PV) field with battery energy storage (BES). Photovoltaic cell capital costs are estimated from NREL's Annual Technology Baseline [33]. Storage costs are obtained from Lazard's Levelized Cost of Storage report and are for Lithium-ion batteries operating in the 'Peaker Replacement' market [34]. Li-ion batteries have a lifetime of approximately 10 years [34], but the LCOE analysis occurs over a 30-year period. It is assumed that the batteries are replaced at the 10^{th} and 20^{th} year of operation, and the total battery cost is discounted appropriately. See Table 6 for the PV+BES cost assumptions.

Table 6: Cost assumptions for a photovoltaic solar array with Lithium-ion battery storage

		Low	Medium	High	Reference
PV capital cost	$\$/kW_e$	1000	1300	1700	[33]
Operations cost	$\$/kW_e$	14	14	14	[22]
Storage capital cost	$\$/kWh_e$	290	350	425	[34]

The PV field was modelling using the 'System Advisor Model' (SAM) [22]. The PV panels are assumed to be one-axis tracking, with total system losses of 14.1%, an inverter efficiency of 96% and a DC-to-AC ratio of 1.2. (These are the default values in SAM). This analysis of the PV field uses the same economic assumptions as the hybrid LCOE calculations and therefore the results are directly comparable.

The battery storage discharges with a power of 2 MW_e. The nominal PV power capacity is also 2 MW_e because the nominal design point of the hybrid plant increases the electrical output by this quantity. However, PV plants have different operational performance than CSP systems. Therefore, the PV field is sized so that it produces the same quantity of energy over the year as the equivalent hybrid plant. As a

This report is available at no cost from the National Renewable Energy Laboratory (NREL) at www.nrel.gov/publications

result, the PV field that corresponds to a solar multiple of 2 has a rated power of 3.225 MW_e and generates 6.98 GWh_e over the course of a year. The PV field that corresponds to a hybrid plant with a solar multiple of 3 has a rated power of 4.82 MW_e and generates 9.34 GWh_e. It is assumed that all the power produced by the PV field can be absorbed by the grid. Thus, no power is curtailed.

The LCOE is calculated for two cases that are equivalent to the hybrid plant operating with solar multiples of 2 and 3, with the "optimal" storage durations of 3 and 10 hours. Results are summarized in

Table 7. When storage is not included PV arrays have similar costs to the hybrid-geothermal system. However, batteries have higher capital costs (290 – 425 $/kWh) and shorter lifetimes (10 years) than thermal storage [34], [35]. Consequently, the LCOE of the hybrid plant with storage is lower than the PV+BES system. For instance, the hybrid plant with σ = 2 and 3 hours of storage has an LCOE of 0.081 ± 0.011 $/kWh, compared to the equivalent PV field value of 0.112 ± 0.024 $/kWh.[1] Similarly, the hybrid plant with σ = 3 and 10 hours of storage has an LCOE of 0.091 ± 0.01 $/kWh, compared to the equivalent PV field value of 0.172 ± 0.035 $/kWh. Given the level of uncertainty, it is fair to assume that there is a compelling economic argument to consider hybrid plants as a competitor to PV systems with batteries. For comparison, other studies have calculated the LCOE of PV-BES to be 0.082 $/kWh [36] for a 200 MW_e solar field with 10 hours of storage, and 0.16 ± 0.05 $/kWh and 0.19 ± 0.05 $/kWh [37] for a 100 MW_e solar field with 3 and 9 hours of storage, respectively.

The quantity of storage was chosen to be "optimal" for the hybrid plant and is unlikely to be the best quantity for the PV field. For instance, the PV field is "better" at producing energy in the winter and at the start and end of the day. Therefore, the PV field can produce the same quantity of energy annually as the hybrid plant without having to increase the size of the field by the same proportion. As a result, the power production profile is less "peaky" and exceeds the threshold for storage to a smaller extent. The stores therefore have lower utilizations and are probably not at their optimal point.

It is worth noting that the concentrating solar field has been assumed to have relatively conservative cost and performance parameters. For instance, the cost of the solar field is 150 $ / m^2, which is higher than costs proposed by some manufacturers. Furthermore, linear Fresnel reflectors typically have poorer optical performance than parabolic trough technologies and thereby produce less energy over the course of a year.

A major factor in the high LCOE of the PV+BES system is the requirement to replace the batteries periodically. In a similar way, HTF in the hybrid plant thermal stores degrades over time and has to be replaced. The above calculations assumed a replacement rate of 1% per year. However, if the plant is operated incorrectly then degradation rates could be higher. For a make-up rate of 10% per year (equivalent to replacing the fluid once every ten years) the LCOE is 0.089 ± 0.011 $/kWh for DPO with 3 hours of storage and $\sigma = 2$, and 0.109 ± 0.012 $/kWh for DPO with 10 hours of storage and $\sigma = 3$, which is still more cost-effective than PV+BES.

[1] These PV+BES LCOE values are averages of those in Table 7.

This report is available at no cost from the National Renewable Energy Laboratory (NREL) at www.nrel.gov/publications

Table 7: LCOE comparison of hybrid geothermal-solar-storage with photovoltaic cells with battery storage. Full results are available in the Supplementary Information.

Annual energy generation, GWh_e	Solar multiple*	Storage duration, h	LCOE, \$ / kWh_e	
			Hybrid plant	PV+BES
6.98	2	0	0.067 ± 0.011	0.062 ± 0.014
		3	0.081 ± 0.011	0.112 ± 0.024
9.34	3	0	0.076 ± 0.012	0.062 ± 0.014
		10	0.091 ± 0.011	0.172 ± 0.035

*For the concentrating solar field

7. Flexible power generation

Storage increases a plant's flexibility as power can be dispatched during hours of greatest demand. Dispatchable power generation is increasingly important as renewable penetration increases. For instance, large quantities of solar power on the Californian grid has led to a surplus of power during the afternoon [38]. This results in the so-called "duck curve" [39], whereby firm capacity must be rapidly dispatched during the evening hours. The abundance of intermittent generation has led to volatile electricity prices, which can even become negative [40]. Consequently, power generation units should be flexible; reducing power delivery during the afternoon and ramping at high slew rates during the evening. Combining baseload production (geothermal) with variable production (CSP) and thermal storage provides the flexibility to operate in such a marketplace. A hybrid system that includes dispatchable storage can provide other benefits to the grid, such as frequency control.

Since dispatchable power generation is a valuable commidity it should be priced accordingly. This section investigates the price that stored energy should be dispatched at for the hybrid system to be economically viable.

The hybrid plant electricity is sold at a flat rate of 0.09 \$/kW_e. Electricity produced by discharging the stores is sold at a multiple of the flat rate, called a "price multiplier." For a system with a given storage duration and solar multiple, the price multiplier required for the system to have an internal rate of return of 10% is calculated. This value of IRR represents a scenario where a system looks profitable. The IRR is calculated using the methodology in [31]; results are presented in Figure 6. The curves indicate that there is an optimal storage size for each plant: as discussed above, small quantities of storage are expensive per kWh and therefore require high price multiples. Increasing the storage size increases the economic return, although extremely large stores are underutilized and again require high-price multiples. For solar multiples of 2, the optimal storage size is around 3 – 4 hours. Increasing the solar multiple increases the optimal storage duration to around 10 hours, as thermal energy availability has increased. Using a synthetic fluid typically requires lower price multipliers to achieve a profitable IRR than mineral oils, which is consistent with the above analysis. Profitable IRRs can be achieved with price multipliers in the region of 1.5 – 1.75

This report is available at no cost from the National Renewable Energy Laboratory (NREL) at www.nrel.gov/publications

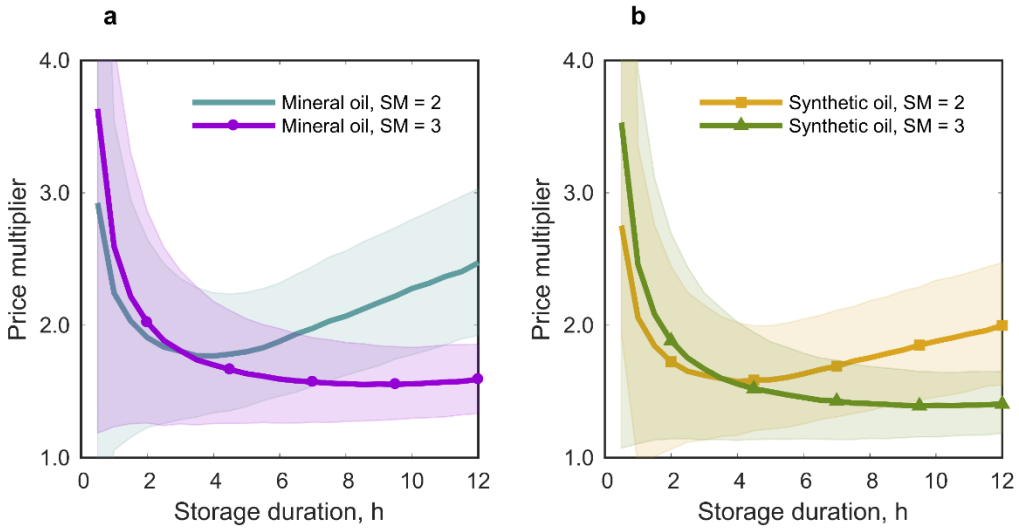

Figure 6: Curves showing the price multiplier required for a hybrid system with a given storage duration to achieve an internal rate of return of 10%. The price multiplier is the increased price that stored energy is dispatched at. Shaded bands show the uncertainty. **a:** Mineral oil storage, with the hot store at 300°C. **b:** Synthetic oil storage, with the hot store at 400°C.

This analysis assumes that all dispatched energy from storage receives the increased price. As such it is not a reflection of the current electricity market where prices vary throughout the day and across the year. In such a scenario, large storage systems may be of little use, since higher prices may only be available for 1 or 2 hours of the day (and may coincide with times of high solar availability). Analyzing this scenario requires time of delivery pricing (including estimates for future years) as well as a control system for the optimal dispatch of storage. This analysis assumes that storage provides value to the grid in various ways that may not be directly quantifiable. Therefore, the 'price multipliers' reflect the average price that stored energy must be dispatched at for the system to be viable.

8. Alternative storage systems

Two-tank liquid stores are the most readily deployable storage system for CSP plants, but several other pre-commercial storage technologies exist that are more compact and cost effective. Options include solid sensible storage, phase change materials (PCMs) or thermochemical storage [41]. Solid sensible storage is currently the most cost-effective option with the lowest technological complexity [42] and includes concrete blocks to which heat is transferred through pipes [43] or packed beds—a storage vessel filled with solid particles through which the HTF percolates [44], [45].

The volume V of the packed bed can be found from

$$E = \beta\left(1-\varepsilon\right)\rho_s V\left[\left(c_s T\right)_h - \left(c_s T\right)_c\right] \tag{15}$$

ρ_s is the solid density, c_s is the solid heat capacity, and ε is the void fraction (the fraction of space not filled by particles), T is the temperature, and β is a simple factor that accounts for the fact that the thermal

This report is available at no cost from the National Renewable Energy Laboratory (NREL) at www.nrel.gov/publications

front in the store is not a step function but has a finite gradient. This means that the full storage is not utilized and should be oversized in order to store the required volume. Subscripts *h* and *c* refer to the hot and cold temperatures, respectively.

The packing material is an iron oxide such as magnetite (Fe_3O_4) with an average c_s = 800 kJ / kg K, ρ_s = 5000 kg/m^3, ε = 0.4 and β = 0.75. The cost of the packing is estimated to be 500 \$ / m^3 [46], and the pressure vessel cost is calculated with the correlations in Appendix B, and uses DPO as the HTF.

Two-tank liquid storage with 4 hours of discharge (32 MWh) operating between 400°C and 190°C requires each tank to have a volume of 330 m^3 and a total capital cost of 39 \$/kWh. However, a packed bed with the same energy capacity and operating temperatures would be 315 m^3 and 14 \$/kWh. Moreover, the HTF volume is reduced from 300 m^3 to 126 m^3, thereby reducing the severity of fire risk. However, the discharging temperature varies with time and the round-trip efficiency may be affected by irregular charge and discharge cycles [47]. Numerous schemes have been proposed to mitigate these problems (such as the inclusion of PCMs [48]), the segmentation of the bed into layers [49]–[51], or mixing the discharging flow with a cooler fluid to control the mixture's temperature. Evaluating the influence of this transient behavior on the integrated plant performance will determine the true cost savings.

9. Conclusions

In this article we investigate how an existing double-flash geothermal power plant can be retrofitted with concentrating solar power to increase the power generation. Five methods of integrating solar heat were studied and the most suitable approach involves reheating the brine after the first flash tank. The solar heat added to this brine is converted to electricity with an efficiency of 24.3%. This approach has a reduced risk of depositing minerals on the heat exchangers or pipework compared to other methods. Retrofitting in this way may be cost effective since the existing power block, pipework, and condenser can be used. Various other approaches exist, such as using solar heat to power a high-temperature topping cycle [52]. Heat could be rejected into the geothermal plant to improve generation. A topping cycle will increase the capital cost but will achieve higher efficiencies. Furthermore, storage systems at higher temperatures are likely to be more compact and cost effective.

Incorporating two-tank liquid thermal storage into the hybrid plant increases the flexibility of the plant, at increased capital cost. Increasing the temperature difference across the tanks reduces the volume and thus the cost. This is an effective approach even if more expensive storage fluids and pressurized vessels are required. The LCOE was calculated for several storage durations and solar field sizes, and was found to be significantly lower than equivalently sized photovoltaic arrays with battery storage because thermal stores are cheaper and have longer lifetimes than batteries. Concrete stores and packed-beds are likely to provide cheaper, more compact storage than liquid tanks, albeit at increased complexity and risk.

Storage provides numerous benefits to the grid, and can dispatch power at times of high electricity prices. Calculations indicate that the price needs to be roughly double the typical flat-rate price of 0.09 \$/kW$_e$ for storage to provide internal rate of returns over 10%. These price points are small compared to the price fluctuations that are currently observed in the Californian energy market. However, exploiting price differentials may not be an option for some current geothermal plant operators if they are committed to an existing power purchase agreement which specifies a fixed electricity price.

This report is available at no cost from the National Renewable Energy Laboratory (NREL) at www.nrel.gov/publications

Acknowledgements

This work was supported by the U.S. Department of Energy under Contract Number DE-AC36-08GO29308 to the National Renewable Energy Laboratory (NREL). The authors gratefully acknowledge Mike Erbes for assisting with the off-design steam turbine modeling and the Naval Geothermal Program Office, including Andrew Sabin, David Meade, Michael Lazaro, and Kelly Blake, for their contributions.

Nomenclature

Roman symbols

c_p	Specific heat capacity, kJ/kg.K
C_{cap}	Capital cost, $
E	Energy, kJ
H	Enthalpy, kJ/kg
$\dot{m}$	Mass flow rate, kg/s
M	Annual operations cost, $
p	Pressure, bar
P	Power, W
$\dot{Q}$	Heat, W
s	Entropy, kJ/kg.K
t	Time, s
T	Temperature, °C
V	Volume, m^3
$\dot{W}$	Work, W

Greek symbols

A	Average absorptance
B	Oversizing of storage tanks
Γ	Intercept factor
E	Packed bed void fraction
η_1	First law efficiency, see Eq. 12
η_{opt}	Optical efficiency, %
η_{sol}	Solar efficiency, see Eq. 13
$\theta_{\perp}, \theta_{\square}$	Transversal and longitudinal incidence angles
P	Reflectance
$\rho_{f,s}$	Fluid or solid density, kg/m^3
Σ	Solar multiple
T	Transmittance
τ_d	Discharging time of stores, s
ϕ	Heat loss, W/m

Abbreviations

FCR	Fixed charge rate
IAM	Incidence angle modifier
IRR	Internal rate of return
LCOE	Levelized cost of electricity, see Eq. 14

Subscripts and superscripts

h,c	Hot and cold
in, out	Inlet and outlet flows

This report is available at no cost from the National Renewable Energy Laboratory (NREL) at www.nrel.gov/publications

Appendix A: Proof showing 1st law efficiency can decrease as solar heat is added

The first law efficiency of a system with no solar heat input is

$$\eta_{1,o} = \frac{W_o}{Q}$$

The first law efficiency of the hybrid plant including a solar heat input is

$$\eta_1 = \frac{W}{Q + Q_{\text{sol}}}$$

The solar conversion efficiency is

$$\eta_{\text{sol}} = \frac{W - W_o}{Q_{\text{sol}}}$$

The first law may therefore be written as

$$\eta_1 = \frac{W + \eta_{\text{sol}} Q_{\text{sol}}}{Q + Q_{\text{sol}}}$$

Differentiating with respect to Q_{sol} leads to

$$\frac{\partial \eta_1}{\partial Q_{\text{sol}}} = \frac{\eta_{\text{sol}} Q - W_o}{\left(Q + Q_{\text{sol}}\right)^2}$$

In order for the first law efficiency to increase with solar heat addition, the first derivative must be greater than zero, this leads to the condition

$$\eta_{\text{sol}} > \frac{W_o}{Q} = \eta_{1,o}$$

Appendix B: Cost Correlations

Cost correlations for storage vessels: The pressure vessel contains the storage media. Pressure vessel cost estimates were obtained from PCL construction by Coso Operating Company and fitted well with a correlation derived from Peters and Timmerhaus [53] (when costs were inflated to current values) for unpressurised vessels. The cost of the vessel depends on its volume V and is given by:

$C_{ves} = 7351 V^{0.557}$

This report is available at no cost from the National Renewable Energy Laboratory (NREL) at www.nrel.gov/publications

Pressurizing the store significantly increases the cost, and the following correlation was obtained from EconExpert [54] (an online tool for capital cost estimation) for pressures over 7 bar:

$C_{pres} = 0.922 + 0.0335P - 0.0003P^2 + 1 \times 10^{-6} P^3$

The total cost of the pressure vessel is therefore given by $C_{PV} = C_{pres}\, C_{ves}$.

Cost correlations for heat exchangers: Correlations from EconExpert for a floating-head, shell-and-tube heat exchanger constructed from carbon steel.

$$C_{HX} = \beta(18944.44 + 280.71A - 0.06601A^2)$$

$$\beta = 1 \text{ for } P < 10 \text{ bar}$$
$$\beta = 1.0011 + 0.001P \text{ for } P \geq 10 \text{ bar}$$

where P is the pressure, and A is the heat transfer area. A is calculated using the log-mean temperature difference method, where

$$A = \frac{Q}{U \,.\, \text{LMTD}}$$

where Q is the heat transferred, U is the overall heat transfer coefficient (assumed to have a constant value of 1000 W / m^{2}K) and LMTD is the log-mean temperature difference, given by

$$\text{LMTD} = \frac{\Delta T_h - \Delta T_c}{\log(\Delta T_h) - \log(\Delta T_c)}$$

where ΔT_h is the temperature difference on the hot side of the heat exchanger, and ΔT_c is the temperature difference on the cold side of the heat exchanger.

Solar field costing: The solar field cost is assumed to be in the range of 100 – 200 \$ / m^2 following discussions with solar collector manufacturers.

HTF costing: Following contact with manufacturers and suppliers, Xceltherm 600 was priced at 2.5 \$/kg and Therminol VP1 was priced at 3.1 \$/kg for bulk quantities (over 19 m^3 or 5000 gallons). The HTF degrades over time, and is replaced at a rate of 1% per year over the lifetime of the plant.

Pump costing: This correlation was derived from EconExpert for a centrifugal pump made from cast steel. P is the discharge pressure, and W is the rated power.

$$C_{pump} = 5648.8 P^{0.4305} \dot{W}^{0.4121}$$

Price of electricity: The price of electricity was set at 0.09 \$ / kWh, following discussions with industrial partners.

Sensitivity analysis: The cost of each component was assumed to follow a normal distribution $C \sim N(\mu, \sigma^2)$, which was truncated to prevent negative costs. A Monte Carlo simulation with 10,000 runs was undertaken. For each run, each component normal distribution was sampled, and the economic metrics evaluated to develop a distribution of costs. The mean value of each distribution was that given by the equations above. The value of the standard deviations is given in Table 8.

This report is available at no cost from the National Renewable Energy Laboratory (NREL) at www.nrel.gov/publications

Table 8: Parameters used in sensitivity analysis

	Mean value, $	Standard deviation	Upper limit	Lower limit
Solar field	150	0.20 μ	10 μ	0.30 μ
HTF	-	0.10 μ	5.0 μ	0.30 μ
Pressure vessel	-	0.25 μ	20 μ	0.30 μ
Heat exchanger	-	0.20μ	10 μ	0.30 μ
Pump	-	0.20 μ	10 μ	0.30 μ
Electricity price	0.09	0.20 μ	1.50 μ	0.20 μ

Dash indicates costs are calculated from correlations above.

Economic assumptions: Economic parameters for calculating the LCOE and IRR are summarized in Table 9 and are the default values used in the System Advisor Model (SAM).

Table 9. Economic factors used in LCOE calculations

Economic parameters	Assumed values
Tax rate, T, %	40
Inflation rate, i, %	2.5
Project debt fraction, d, %	60
Internal rate of return, IRR, %	10
Nominal debt interest rate, NINT, %	8
Depreciation rate, D_j , %	20, 32, 20, 14, 14; 0 thereafter

This report is available at no cost from the National Renewable Energy Laboratory (NREL) at www.nrel.gov/publications

References

[1] D. S. Wendt and G. L. Mines, "Use of a Geothermal-Solar Retrofit Hybrid Power Plant to Mitigate Declines in Geothermal Resource Productivity," *Transactions of the GRC,* vol. 38, 2014.

[2] D. M. Snyder, K. F. Beckers, K. R. Young, and B. Johnston, "Analysis of Geothermal Reservoir and Well Operational Conditions using Monthly Production Reports from Nevada and California," *Transactions of the GRC,* vol. 41, 2017.

[3] D. S. Wendt and G. L. Mines, "Stillwater Hybrid Geo-Solar Power Plant Optimization Analyses," *Geotherm. Resour. Counc. 39th Annu. Meet.*, vol. 39, pp. 891–900, 2015.

[4] G. Dimarzio, L. Angelini, W. Price, C. Chin, and S. Harris, "The Stillwater Triple Hybrid Power Plant: Integrating Geothermal, Solar Photovoltaic and Solar Thermal Power Generation," in *Proceedings World Geothermal Congress*, 2015, no. April, pp. 1–5.

[5] O. C. Kuyumcu, O. S. C. C. Özalevli, D. K. Baker, and S. K. Somek, "Design and Implementation of the Gümüşköy Hybrid Geothermal and Solar Thermal Power System," *Trans. - Geotherm. Resour. Counc.*, vol. 38, pp. 811–816, 2014.

[6] C. Zhou, E. Doroodchi, and B. Moghtaderi, "An in-depth assessment of hybrid solar – geothermal power generation," *Energy Convers. Manag.*, vol. 74, pp. 88–101, 2013.

[7] M. Ayub, A. Mitsos, and H. Ghasemi, "Thermo-economic analysis of a hybrid solar-binary geothermal power plant," *Energy*, vol. 87, pp. 326–335, 2015.

[8] F. Heberle, M. Hofer, N. Ürlings, H. Schr, T. Anderlohr, and D. Brüggemann, "Techno-economic analysis of a solar thermal retrofit for an air-cooled geothermal Organic Rankine Cycle power plant," *Renew. Energy*, vol. 113, pp. 494–502, 2017.

[9] A. Lentz and R. Almanza, "Solar – geothermal hybrid system," *Appl. Therm. Eng.*, vol. 26, pp. 1537–1544, 2006.

[10] S. Handal, Y. Alvarenga, and M. Recinos, "Geothermal steam production by solar energy," *Geotherm. Resour. Counc. 31st Annu. Meet.*, vol. 31, 2007.

[11] Y. Alvarenga, S. Handal, and M. Recinos, "Solar steam booster in the Ahuachapan geothermal field," *Geotherm. Resour. Counc. 32nd Annu. Meet.*, vol. 32, 2008.

[12] J. Miguel Cardemil, F. Cortés, A. Díaz, and R. Escobar, "Thermodynamic evaluation of solar-geothermal hybrid power plants in northern Chile," *Energy Convers. Manag.*, vol. 123, pp. 348–361, 2016.

[13] SimTech, "Process Simulation Environment (IPSEpro)." 2017.

[14] R. Dipippo, *Geothermal power plants*, 4th edition. Butterworth-Heinemann, 2016.

[15] L. S. Dixon and C. A. Hall, *Fluid Mechanics and Thermodynamics of Turbomachinery*. Elsevier Science, 2010.

This report is available at no cost from the National Renewable Energy Laboratory (NREL) at www.nrel.gov/publications

[16] D. H. Cooke, “On Prediction of Off-Design Multistage Turbine Pressures by Stodola’s Ellipse 1,” *J. Eng. Gas Turbines Power*, vol. 107, pp. 596–606, 1985.

[17] J. D. Denton, “Loss mechanisms in Turbomachines,” *J. Turbomach.*, vol. 115, no. October 1993, 2017.

[18] R. C. Spencer, K. C. Cotton, and C. N. Cannon, “A method for predicting the performance of steam turbine-generators 16,500 kW and larger,” 1974.

[19] L. C. Fuller and T. K. Stovall, “A computer code for the performance of regenerative superheated steam-turbine cycles,” in *ORNL-5547, NASA CR-159540*, 1979.

[20] Y. K. Choo and P. J. Staiger, “New Features and Applications of PRESTO , a Computer Code for the Performance of Regenerative , Superheated Steam Turbine Cycles,” in *NASA TP 1954 c.1*, 1982.

[21] H. Lazalde-Crabtree, “Design approach of steam-water separators and steam dryers for geothermal applications,” in *Geothermal Resources Council Bulletin*, 1984.

[22] NREL, “System Advisor Model (SAM).” 2017.

[23] G. Zhu, “Development of an analytical optical method for linear fresnel collectors,” *Sol. Energy*, vol. 94, pp. 240–252, 2013.

[24] G. Zhu and C. Turchi, “Solar Field Optical Characterization at Stillwater Geothermal / Solar Hybrid Plant,” *J. Sol. Energy Eng.*, vol. 139, no. June, pp. 1–10, 2017.

[25] F. Burkholder and C. F. Kutscher, “Heat loss testing of Schott’s 2008 PTR70 parabolic trough receiver,” 2009.

[26] J. McTigue, J. Castro, G. Mungas, N. Kramer, J. King, and C. Turchi, “Retrofitting a Geothermal Plant with Solar and Storage to Increase Power Generation,” *Trans. GRC*, vol. 41, 2017.

[27] E. González-Roubaud, D. Pérez-Osorio, and C. Prieto, “Review of commercial thermal energy storage in concentrated solar power plants : Steam vs . molten salts,” *Renew. Sustain. Energy Rev.*, vol. 80, no. March 2016, pp. 133–148, 2017.

[28] P. N. Mathur, “An assessment of solar-geothermal hybrid system concepts,” 1979.

[29] Y. Nakao, Y. Mugikura, K. Ogata, and N. Katsuki, “Development of Hybrid Geothermal Power Plants in Japan,” in *Transactions - Geothermal Resources Council*, 2017, vol. 41.

[30] Y. Kawahara *et al.*, “Laboratory experiments on prevention and dissolution of silica deposits in a porous column (1): Solid deposition due to silica particle aggregation and inhibition by acid dosing,” *Trans. - Geotherm. Resour. Counc.*, vol. 36, pp. 1–4, 2012.

[31] W. Short and D. J. Packey, “A Manual for the Economic Evaluation of Energy Efficiency and Renewable Energy Technologies,” no. March, 1995.

[32] P. Denholm, J. Eichman, and R. Margolis, “Evaluating the Technical and Economic Performance of PV Plus Storage Power Plants,” Technical report NREL/TP-6A20-68737, 2017.

This report is available at no cost from the National Renewable Energy Laboratory (NREL) at www.nrel.gov/publications

[33] NREL, “2017 Annual Technology Baseline.” 2017.

[34] Lazard, “Lazard’s Levelized Cost of Storage Analysis - Version 3.0,” 2017.

[35] D. Newbery, “Shifting demand and supply over time and space to manage intermittent generation: The economics of electrical storage,” *Energy Policy*, vol. 113, no. November 2017, pp. 711–720, 2018.

[36] Lazard, “Levelized Cost of Energy Analysis - version 11.0,” 2017.

[37] D. Feldman, R. Margolis, J. Stekli, D. Feldman, R. Margolis, and J. Stekli, “Exploring the Potential Competitiveness of Utility-Scale Photovoltaics plus Batteries with Concentrating Solar Power , 2015 – 2030,” NREL Technical Report TP-6A20-66592, 2016.

[38] R. Fu, D. Feldman, R. Margolis, M. Woodhouse, and K. Ardani, “U.S. Solar Photovoltaic System Cost Benchmark : Q1 2017,” NREL Technical Report TP-6A20-68925, 2017.

[39] P. Denholm, M. O. Connell, G. Brinkman, and J. Jorgenson, “Overgeneration from Solar Energy in California : A Field Guide to the Duck Chart,” Technical report NREL/TP-6A20-65023, 2015.

[40] California ISO, “California ISO Q3 2017 Report on Market Issues and Performance,” 2017.

[41] P. Pardo, A. Deydier, Z. Anxionnaz-Minvielle, S. Roug??, M. Cabassud, and P. Cognet, “A review on high temperature thermochemical heat energy storage,” *Renew. Sustain. Energy Rev.*, vol. 32, pp. 591–610, 2014.

[42] H. Zhang, J. Baeyens, G. Caceres, J. Degreve, and Y. Lv, “Thermal energy storage: Recent developments and practical aspects,” *Prog. Energy Combust. Sci.*, vol. 53, pp. 1–40, 2016.

[43] D. Laing, W. D. Steinmann, P. Viebahn, F. Gräter, and C. Bahl, “Economic Analysis and Life Cycle Assessment of Concrete Thermal Energy Storage for Parabolic Trough Power Plants,” *J. Sol. Energy Eng.*, vol. 132, no. 4, p. 41013, 2010.

[44] G. Zanganeh, a. Pedretti, S. Zavattoni, M. Barbato, and a. Steinfeld, “Packed-bed thermal storage for concentrated solar power – Pilot-scale demonstration and industrial-scale design,” *Sol. Energy*, vol. 86, no. 10, pp. 3084–3098, Oct. 2012.

[45] J. McTigue and A. White, “A comparison of radial-flow and axial-flow packed beds for thermal energy storage,” *Appl. Energy*, 2017.

[46] J. McTigue, “Analysis and optimisation of thermal energy storage,” University of Cambridge PhD thesis, 2016.

[47] A. Bruch, J. F. Fourmigué, and R. Couturier, “Experimental and numerical investigation of a pilot-scale thermal oil packed bed thermal storage system for CSP power plant,” *Sol. Energy*, vol. 105, pp. 116–125, 2014.

[48] G. Zanganeh, M. Commerford, A. Haselbacher, A. Pedretti, and A. Steinfeld, “Stabilization of the outflow temperature of a packed-bed thermal energy storage by combining rocks with phase change materials,” *Appl. Therm. Eng.*, vol. 70, no. 1, pp. 316–320, Sep. 2014.

This report is available at no cost from the National Renewable Energy Laboratory (NREL) at www.nrel.gov/publications

[49] D. M. Crandall and E. F. Thacher, “Segmented thermal storage,” *Sol. Energy*, vol. 77, no. 4, pp. 435–440, Oct. 2004.

[50] A. J. White, J. D. McTigue, and C. N. Markides, “Analysis and optimisation of packed-bed thermal reservoirs for electricity storage applications,” *Proc. Inst. Mech. Eng. Part A J. Power Process Eng.*, vol. 230, no. 7, pp. 739–754, 2016.

[51] J. D. McTigue and A. J. White, “Segmented packed beds for improved thermal energy storage performance,” *IET Renew. Power Gener.*, vol. 10, no. 10, pp. 1498–1505, 2016.

[52] N. Bonyadi, E. Johnson, and D. Baker, “Technoeconomic and exergy analysis of a solar geothermal hybrid electric power plant using a novel combined cycle,” *Energy Convers. Manag.*, vol. 156, no. September 2017, pp. 542–554, 2018.

[53] M. S. Peters and K. D. Timmerhaus, *Plant design and economics for chemical engineers*. McGraw-Hill, Inc., 1990.

[54] P. T. Vasudevan and T. Ulrich, “EconExpert,” 2000. [Online]. Available: http://www.ulrichvasudesign.com/cgi-bin/cgiwrap.cgi/econ/econnew.pl. [Accessed: 24-Jan-2018].

[55] “National Solar Radiation Database.” [Online]. Available: https://nsrdb.nrel.gov/. [Accessed: 12-Nov-2017].

This report is available at no cost from the National Renewable Energy Laboratory (NREL) at www.nrel.gov/publications